Electronic Supplementary Material (ESI) for RSC Advances.

Supporting Information

Very Fast Hot Carrier Diffusion in Unconstrained MoS_2 on Glass Substrate: Discovered by Picosecond ET-Raman

Pengyu Yuan,[†,§] Hong Tan,[‡,§] Ridong Wang,[†] Tianyu Wang,[†] Xinwei Wang[*,†]

[†] Department of Mechanical Engineering, Iowa State University, Ames, IA 50011, USA.

[‡] School of Energy and Power Engineering, Nanjing University of Science and Technology, Nanjing, Jiangsu 210094, China.

[§]These authors contributed equally to this work.

[*] Corresponding author. Tel: 001-515-294-8023, Email: xwang3@iastate.edu

Contents

S1. Picosecond ET-Raman Experimental Details S3
S2. MoS_2 Nanosheets Sample Supported on Glass Substrate Preparation S3
S3. ET-Raman Experiment Results Summary S7
S4. 3D Numerical Simulation Model and Data Reduction Details S8
S5. Theoretical Raman Intensity Calculation S12
References S14

S1. Picosecond ET-Raman Experimental Details

We perform the Raman experiments by using a confocal Raman system that consists of a Raman spectrometer (Voyage™, B&W Tek, Inc.) and a microscope (Olympus BX53). The 532 nm CW laser or ps laser is introduced to the Raman system and the laser power is adjusted by a motorized neutral-density (ND) filter system (CONEX-NSR1 and NSND-5, Newport Corporation). The laser source could be switched by the flip mounted mirror before it enters the Raman system without any other change in the experiment setup. We use a 3D piezo-actuated nano-stage (MAX313D, Thorlabs, Inc.) which has a resolution of ~5 nm to search for and identify the MoS_2 sample under the microscope. This stage is also used in the Raman shift mapping experiment and it provides us accurate step size. The laser beam is focused on a specific area of the samples (as shown in Fig. 3). During the experiments, a LabVIEW-based program is applied to fully control the Raman spectrometer, the motorized ND filter, and 3D nano-stage. The Raman spectrometer could automatically acquire and store the spectrum for each energy level after the ND filter is set or each position after the 3D nano-stage is set during the mapping Raman experiment. This significantly shortens the experiment time, reduces the external disturbance, and therefore improves the precision and accuracy of the experiments. By analyzing the Raman spectrum, we could evaluate the RSC of MoS_2. Based on the RSC under different heating states, we can directly determine the hot carrier diffusivity and interfacial thermal resistance.

S2. MoS_2 Nanosheets Sample Supported on Glass Substrate Preparation

The MoS_2 samples used for this study are natural occurring crystals from SPI Supplies (429MS-AB, molybdenum disulfide). Six few-layered MoS_2 samples are prepared by using a

micromechanical exfoliation technique with adhesive tape and gel film to obtain a relative flat, clean, and fresh surface. The samples are mounted on the glass substrate (Fisher brand pre-cleaned microscope slide). An optical microscope, atomic force microscope (AFM) and Raman spectroscopy are used to identify and locate the MoS_2 nanosheets. The MoS_2 nanosheets have the lateral size ranging from 7 to 16 μm. Compared to the c-Si substrate, MoS_2 nanosheets on glass substrate have better optical contrast,[1] so we could quickly identify larger ultrathin sheets.

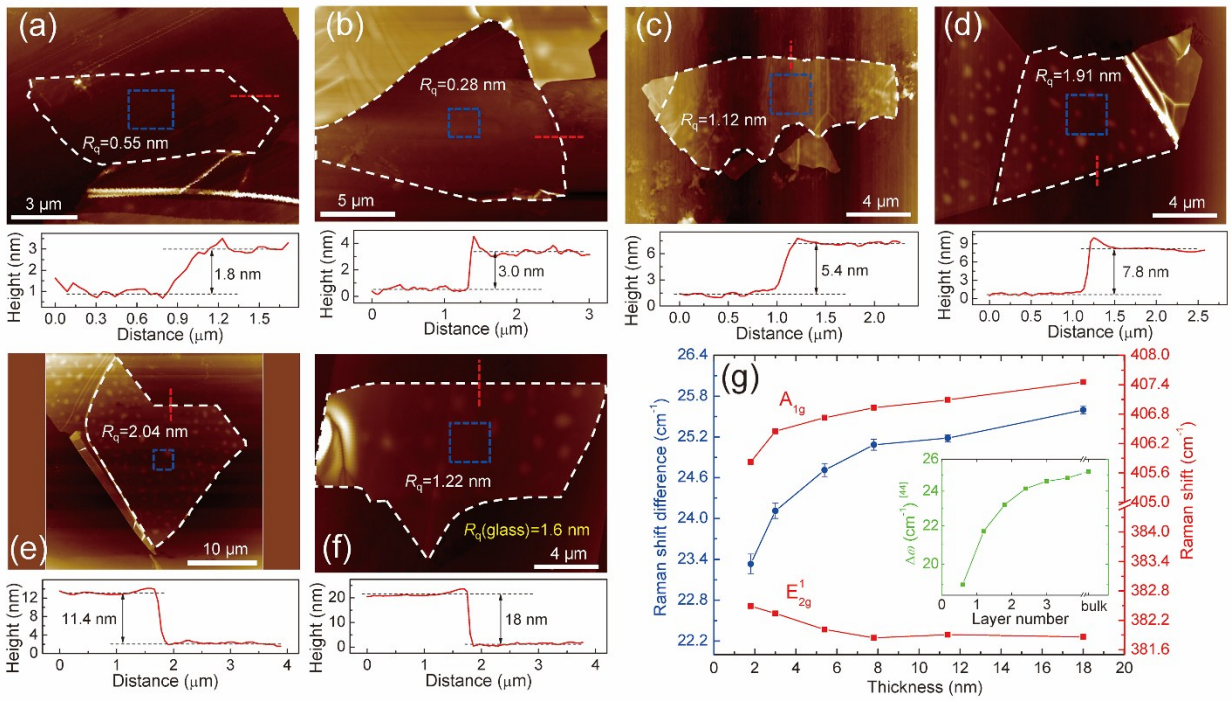

Figure. S1 (a)-(f) AFM measurement results of six MoS_2/glass samples. The upper images in (a)-(f) show the AFM images. The white dashed circled area indicates the measured MoS_2 sample. The blue dashed box indicates the area where ET-Raman experiment is performed. The height profiles under the AFM images show the height measurement along the red dashed lines in the above AFM images. The R_q value in each AFM image indicates the RMS roughness of MoS_2. R_q (glass) in (f) shows the RMS roughness of the glass substrate. (g) Thickness dependence of Raman shift of two Raman modes from MoS_2 nanosheets (right vertical axis) and

their difference (left vertical axis). The two modes shift away from each other with increased thickness. The inset shows the results and prediction based on Lee *et al.*'s work.[2]

Figure S1 (a)-(g) show AFM images of the six MoS_2 samples on glass substrate. In each image, we use the dashed white circle to mark the sample area; the red dashed line to indicate the height profiles measurement area and the result is shown beneath the AFM image. The samples have a thickness of 1.8 nm, 3.0 nm, 5.4 nm, 7.8 nm, 11.4 nm, and 18 nm, respectively. Take the 1.8 nm thick MoS_2 for example, it has a surface roughness (R_q) [Root Mean Square average of height deviations (Δz) taken from the mean area data plane, expressed as $\sqrt{\sum z_i / N}$] of 0.55 nm. Also, the substrate (glass) has a R_q (glass) around 1.6 nm which is pretty large compared with the c-Si substrate we used in previous works (R_q is only 0.09 nm). This is because that the glass substrate is not polished. The higher roughness could also suggest the wrinkles or ripples in the samples. The white dots could be the gel film residues introduced from the MoS_2 sample preparation process because of the high points of the glass substrate. During the sample transfer process (from gel film to glass substrate), the MoS_2 film could only have good contact with the high points of glass, and this attraction is stronger than that between MoS_2 film and the gel film. However, the suspended area (no high point support) of the MoS_2 film has a much weaker attraction with the glass. So the residues from gel film could be easily left on the MoS_2 film surface when the gel film detaches. For the thick samples, the interlayer van der Waals interaction within the MoS_2 film is very strong compared to the attraction between MoS_2 and gel film. But, for the ultrathin samples (1.8 nm has only three atomic layers), the final MoS_2 film sample on glass experiences one last exfoliation when the gel film detaches it. Around half of the MoS_2 film is taken away by the gel film instead of being fully released to the glass substrate. So the thin sample surface is free of residue from the gel film.

Besides, compared with the hydrophobic silicon, the glass is hydrophilic and large numbers of water molecules may be introduced to the interface. For the thick samples, the white dots are more evident and dense. We speculate that the water molecules could permeate through the thinner MoS_2 nanosheets more easily and evaporate into the environment. The surficial water could also affect the samples' thermal and electrical properties. Figure S1 (g) shows the thickness dependence of Raman shift of two Raman modes of MoS_2. The Raman shift difference between E^1_{2g} and A_{1g} modes becomes larger with increased sample thickness, and this is widely used to determine the layer number of MoS_2 nanosheets.[2] So we also plot $\Delta\omega$ as a function of the sample thickness. It is confirmed that $\Delta\omega$ increases with the thickness of MoS_2. Our results agree well with results and predictions of Lee *et al.*'s work[2] which validates our AFM measurement results.

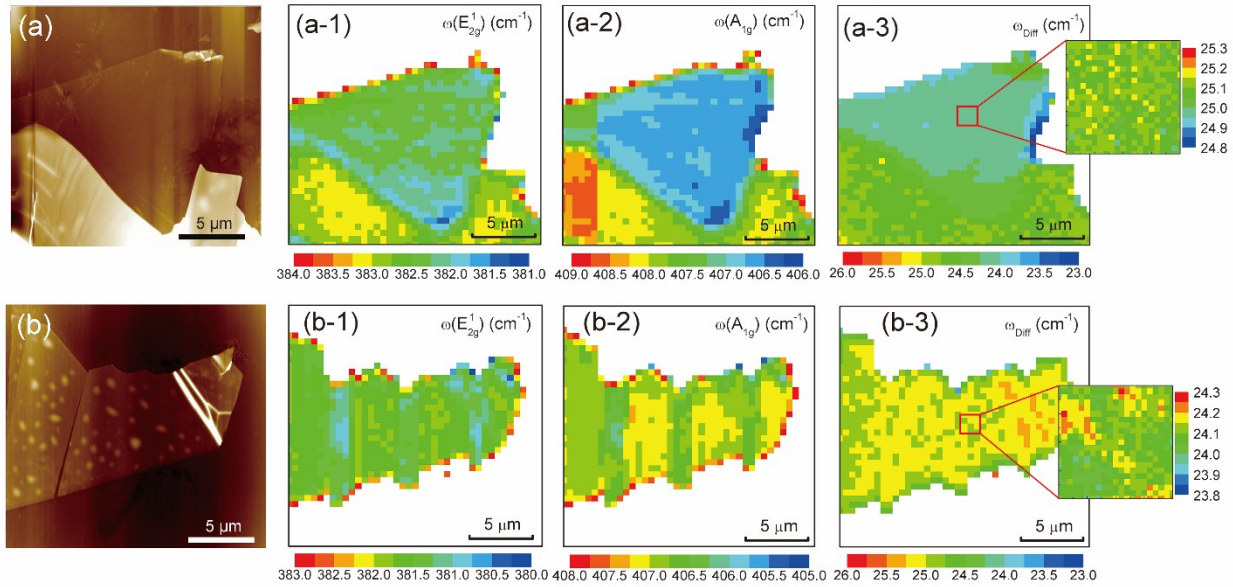

Figure. S2 False color images of Raman shift mapping of 3.0 nm and 7.8 nm thick MoS_2 samples. The Raman shift mappings from E^1_{2g} mode are shown in (a-1) and (b-1), from A_{1g}

mode are shown in (a-2) and (b-2). (a-3) and (b-3) show the Raman shift difference between these two modes. The red squares in (a-3) and (b-3) mark the smaller area for detailed mapping as shown in the enlarged view. The small variance of ω_{Diff} confirms the samples' uniform thickness.

To have a better idea of the uniformity of sample surface structure, we also do the Raman shift mapping by using CW laser line for the 3.0 nm and 7.8 nm thick MoS_2 samples. Here we take the 3.0 nm thick MoS_2 sample for instance to discuss the Raman mapping results. Figure S2 (a) shows its AFM image with a width of 20 μm. The Raman spectra are recorded for each point with a step size of 500 nm and then they are analyzed by a MATLAB-based automatic fitting program to determine the Raman shift information. Figure S2 (a-1) and (a-2) show the false color images created from the Raman shift of E^1_{2g} and A_{1g} modes as a function of position. Figure S2 (a-3) shows the Raman shift difference between these two modes. Because we did the Raman experiments for *D* and *R* determination on a small area of the sample, to gather more information of that area, we zoom in the mapping area as marked with red square in Fig. S2 (a-3). In the enlarged view, the mapping step size for this area is 100 nm. The relatively small variance of Raman shift difference mapping confirms the uniform sample thickness. In the mapping result of the samples, the boundary does not have a smooth transition. We attribute this to the possible real structure variance. Besides, as just discovered in our group, the asymmetry of Raman scattering by structure variation could also account for this result.[3]

S3. ET-Raman Experiment Results Summary

Table S1. Summary of Raman experiment results of six MoS_2 samples. The steady-state Raman shift power coefficient (RSC) values under 20× and 100× objective with CW laser (χ_{CW1} and

χ_{CW2}) for E^1_{2g} mode of MoS_2. The zero-transport state RSC values under 50× and 100× objectives with ps laser (χ_{ps1} and χ_{ps2}). Also the normalized RSC (Θ_1 and Θ_2).

Sample thickness (nm)	**1.8 nm**	**3.0 nm**	**5.4 nm**	**7.8 nm**	**11.4 nm**	**18.0 nm**
Band gap (eV)	1.64	1.54	1.42	1.35	1.31	1.30
χ_{CW1} (cm^{-1}/mW)	-(0.289±0.009)	-(0.344±0.014)	-(0.289±0.009)	-(0.370±0.017)	-(0.369±0.017)	-(0.240±0.010)
χ_{CW2} (cm^{-1}/mW)	-(0.960±0.043)	-(0.940±0.041)	-(0.973±0.040)	-(0.936±0.044)	-(0.784±0.032)	-(0.620±0.023)
χ_{ps1} (cm^{-1}/mW)	-(1.85±0.11)	-(1.43±0.03)	-(1.24±0.02)	-(1.10±0.04)	-(0.71±0.02)	-(0.42±0.01)
χ_{ps2} (cm^{-1}/mW)	-(3.77±0.08)	-(3.09±0.06)	-(2.72±0.08)	-(2.04±0.06)	-(1.48±0.02)	-(1.05±0.02)
Θ_1	-(0.150±0.010)	-(0.207±0.010)	-(0.251±0.014)	-(0.394±0.025)	-(0.375±0.017)	-(0.382±0.021)
Θ_2	-(0.499±0.038)	-(0.566±0.030)	-(0.658±0.034)	-(1.00±0.06)	-(1.03±0.05)	-(0.988±0.053)

S4. 3D Numerical Simulation Model and Data Reduction Details

From the Raman spectroscopy, the evaluated temperature rise of the sample is Raman/laser intensity weighted over the laser spot size for CW laser heating, and also time averaged over the pulse duration for ps laser heating. So we express the temperature rises as:

$$\overline{T}_{CW} = \int_0^{V_0} I_a(r,z)T(r,z)dv \Big/ \int_0^{V_0} I_a(r,z)dv, \tag{S1}$$

and

$$\overline{T}_{ps} = \int_0^{t_0}\int_0^{V_0} I_a(r,z,t)T(r,z,t)dv \Big/ \int_0^{t_0}\int_0^{V_0} I_a(r,z,t)dv. \tag{S2}$$

For the laser intensity I_a (W/m^3), after considering space and time domain Gaussian distribution

and the Beer-Lambert law, we have

$$I_a(r,z,t) = \frac{I_0}{\tau_L}\exp\left[-\frac{r^2}{r_0^2}\right]\exp\left[-\ln(2)\frac{t^2}{t_0^2}\right]\exp\left[-\frac{z}{\tau_L}\right], \quad \text{(S3)}$$

where I_0 (W/m^3) is the peak laser intensity, r_0 is the laser spot radius, t_0 (6.5 ps) is the half pulse width. $\tau_L = \lambda/4\pi k_L$ is the laser absorption depth. λ=532 nm (the laser wavelength), and k_L is the extinction coefficient. We also take these into account in following 3D numerical modeling data processing.

The model calculation size of the substrate has a radius and thickness of 50 μm. The MoS_2 sample takes its actual size and thickness. The smallest mesh size along the thickness direction is 0.1 nm and increases from the MoS_2 surface to the substrate with an increasing ratio of 1.02. The smallest mesh size is 1 nm in the radial direction and also increases with a ratio of 1.02. In our modeling, in the in-plane and cross-plane directions, we take $k_P = 52$ W/mK [4] and $k_\perp = 2$ W/mK [5] for MoS_2. k_{glass}=1.4 W/mK [6]. P=1 mW is the excitation laser energy before entering the sample for both CW laser and ps laser sources and the laser spot size is identical to the experiment. As considered in our previous work, the MoS_2 nanosheets have the thickness dependent bandgap.[7] As summarized in Table S1, we extract the E_g values to determine R and D values. This consideration is especially important and necessary for relatively thin samples: 1.8 nm MoS_2 has E_g as 1.64 eV, and it dramatically decreases down to 1.42 eV for 5.4 nm. τ is set as 1 ns at room temperature as we did before.[8] We first solve the carrier diffusion equation [eq (1)] and then the heat conduction one with the hot carrier concentration $\Delta N(r,t)$ used in the source term.

When a laser beam irradiates the sample surface, multiple reflections happen at the interface

between MoS_2 and glass. Based on the optical properties of these two materials, we could calculate the total absorpotion rate in MoS_2 as I_0, according to the Transfer Matrix Method (TMM).[9] For glass substrate, we assume there is no laser absorption due to its high transparence. As demonstrated before, compared the ET-Raman technique for using Si substrate, the glass has the advantages to eliminate the errors from the local laser absorption evaluation and temperature coefficient calibration. For glass substrate, we will do following treatment.

The temperature coefficient χ_T is for MoS_2. For steady state CW laser Raman, the temperature rise (K/mW) of MoS_2 is ΔT_1. So we express the temperature rise by Raman shift power coefficient (RSC) as

$$\chi_{\mathrm{CW,\,MoS_2}} = \Delta T_1 \times \chi_{\mathrm{T,\,MoS_2}}. \tag{S4}$$

Because there is no laser absorption in substrate, $\Delta T_1 \propto I_0$ which also has the *R* and *D* effect.

For the zero-transport state ps laser Raman, it is a little more complicated. As mentioned above, for the pulsed laser (ps laser) heating, the temperature rise of the sample is from a single pulse and the steady-state accumulation of the heat. The ps laser has a cooling time (t_c) between pulses around 20.8 ns as shown in Fig. 2(b). And, compared to Si substrate, glass has a smaller thermal conductivity and therefore could not dissipate the heat efficiently.[10] Besides, the thermal diffusion length (L_t) in glass within one repetition period could be estimated as $L_t = 2\sqrt{\alpha_k t_c} = 0.262\ \mu\mathrm{m}$, where α_k is the thermal diffusivity of glass. Scaling this result to the three dimensions, the heat will outspread over a hemisphere of radius L_t after a t_c has elapsed. For example, the temperature of the sample will be cooled down to $\pi \times r_0^2(\text{PS laser}, 50\times) \times L_{\text{thickness}} / (2/3 \times \pi \times L_t^3)$ of its original which is around 3%. As a results,

pulse accumulation effect in this work has to be taken into account.

Considering the single pulse heating (laser absorption from the fast thermalization process) and steady-state accumulation of the heat, we could express the temperature rise (K/mW) of MoS_2 RSC under 50× and 100× objectives as

$$\chi_{\mathrm{ps1,\,MoS_2}} = (\Delta T_2 + \Delta T_\mathrm{s}) \times \chi_{\mathrm{T,\,MoS_2}}, \tag{S5}$$

$$\chi_{\mathrm{ps2,\,MoS_2}} = (\Delta T_3 + \Delta T_\mathrm{s}) \times \chi_{\mathrm{T,\,MoS_2}}, \tag{S6}$$

where $\Delta T_2 \,\&\, \Delta T_3 \propto I_0$. ΔT_s represents the temperature rise from the steady-state accumulation of heat, and it is same for each sample.

From the 3D simulation, for the steady-state CW laser heating, we could get ΔT_1 of MoS_2. From zero-transport state ps laser heating, we could directly get ΔT_2 and ΔT_3 by only considering the laser absorption for single pulse heating. Because the temperature rise difference of ps laser heating between 50× and 100× objective is only a function of the laser absorption of the sample, so does the normalized RSC of MoS_2.

From eqs (S4), (S5), and (S6), we have

$$\Theta_{\mathrm{MoS_2}} = \frac{\chi_{\mathrm{CW,\,MoS_2}}}{\chi_{\mathrm{ps2,\,MoS_2}} - \chi_{\mathrm{ps1,\,MoS_2}}} = \frac{\Delta T_1}{\Delta T_3 - \Delta T_2}. \tag{S7}$$

The term ΔT_1 and $(\Delta T_3 - \Delta T_2)$ are only related to the laser absorption in MoS_2. So the normalized RSC value is now only a function of two parameters: $\Theta(R, D)$. The effect from laser absorption evaluation is successfully ruled out. For each sample, from the 3D numerical simulation and

Raman experiment, we could calculate the normalized RSC (Θ_1 and Θ_2) for MoS_2 in the (D, R) space. Note the temperature rise evaluation from the simulation has considered the temperature distribution in both space and time domain as expressed by eqs (S1) and (S2).

S5. Theoretical Raman Intensity Calculation

The multiple reflections of the incident laser beam and Raman signal within the supported nanosheets has been studied in previous work.[11] The net absorption factor (F_{ab}) is given by

$$F_{ab} = t_1 \frac{(1 + r_2 r_3 e^{-2i\beta_2}) e^{-i\beta_x} + (r_2 + r_3 e^{-2i\beta_2}) e^{-i(2\beta_1 - \beta_x)}}{1 + r_2 r_3 e^{-2i\beta_2} + (r_2 + r_3 e^{-2i\beta_2}) r_1 e^{-2i\beta_1}}, \quad \text{(S8)}$$

where $t_1 = 2n_0/(n_0 + n_1)$, $r_1 = (n_0 - n_1)/(n_0 + n_1)$, $r_2 = (n_1 - n_2)/(n_1 + n_2)$, and $r_3 = (n_2 - n_3)/(n_2 + n_3)$ are Fresnel transmittance and reflection coefficients for the interface involving air (0), MoS_2 (1), air (2), and glass (3). n_0, n_1, n_2 and n_3 are the refractive indices for air, MoS_2, air, and glass, respectively. $\beta_x = 2\pi x n_1/\lambda$, $\beta_1 = 2\pi d_1 n_1/\lambda$ and $\beta_2 = 2\pi d_2 n_2/\lambda$, where x is the depth of the point where interaction occurs, λ is the wavelength of the incident laser (532 nm), d_1 and d_2 are the thickness of MoS_2 nanosheets and glass, respectively. We assume there is no spacing at the interface. The Raman intensity variation with the MoS_2 thickness will be compared with the experimental results.

Similarly, the net scattering factor (F_{sc}) is described by

$$F_{sc} = t_1' \frac{(1 + r_2 r_3 e^{-2i\beta_2}) e^{-i\beta_x} + (r_2 + r_3 e^{-2i\beta_2}) e^{-i(2\beta_1 - \beta_x)}}{1 + r_2 r_3 e^{-2i\beta_2} + (r_2 + r_3 e^{-2i\beta_2}) r_1 e^{-2i\beta_1}}, \quad \text{(S9)}$$

where $t_1' = 2n_1/(n_0 + n_1)$ and λ is the wavelength of the E_{2g}^1 mode of MoS_2. Then we could

express the theoretical Raman intensity (F) of MoS_2 as

$$F = \int_0^{d_1} \left| F_{ab} F_{sc} \right|^2 dx , \tag{S10}$$

In the calculation, the refractive index of different thickness MoS_2 nanosheets is extracted from Yim *et al*.'s work.[7] The refractive indices of glass are 1.48 + 0*i* and 1.47 + 0*i* for incident laser and Raman scattering, respectively.

References

1. G. Rubio-Bollinger, R. Guerrero, D. P. de Lara, J. Quereda, L. Vaquero-Garzon, N. Agraït, R. Bratschitsch and A. Castellanos-Gomez, *Electronics*, 2015, **4**, 847-856.
2. C. Lee, H. Yan, L. E. Brus, T. F. Heinz, J. Hone and S. Ryu, *ACS Nano*, 2010, **4**, 2695-2700.
3. R. Wang, P. Yuan, M. Han, S. Xu, T. Wang and X. Wang, *Opt. Express*, 2017, **25**, 18378-18392.
4. S. Sahoo, A. P. Gaur, M. Ahmadi, M. J.-F. Guinel and R. S. Katiyar, *J. Phys. Chem. C*, 2013, **117**, 9042-9047.
5. J. Liu, G.-M. Choi and D. G. Cahill, *J. Appl. Phys.*, 2014, **116**, 233107.
6. T. L. Bergman and F. P. Incropera, *Fundamentals of Heat and Mass Transfer*, John Wiley & Sons, 2011.
7. C. Yim, M. O'Brien, N. McEvoy, S. Winters, I. Mirza, J. G. Lunney and G. S. Duesberg, *Appl. Phys. Lett.*, 2014, **104**, 103114.
8. H. Shi, R. Yan, S. Bertolazzi, J. Brivio, B. Gao, A. Kis, D. Jena, H. G. Xing and L. Huang, *ACS Nano*, 2013, **7**, 1072-1080.
9. E. X. Pérez, *Design, fabrication and characterization of porous silicon multilayer optical devices*, Universitat Rovira i Virgili, 2008.
10. A. J. Schmidt, X. Chen and G. Chen, *Rev. Sci. Instrum.*, 2008, **79**, 114902.
11. D. Yoon, H. Moon, Y.-W. Son, J. S. Choi, B. H. Park, Y. H. Cha, Y. D. Kim and H. Cheong, *Phys. Rev. B*, 2009, **80**, 125422.